Linear Hybrid Actuator for Active Force Cancellation

D. Laro[1], R. Boshuisen[1], J. Dams[2], J. van Eijk[3,4]

[1]MI-Partners, Dillenburgstraat 9n, Eindhoven, N-Brabant, 5652 AM, the Netherlands
[2]Magnetic Innovations, Oude Kerkstraat 61a, Eindhoven, N-Brabant, 5507 LB, the Netherlands
[3]TU Delft, Mekelweg 2, Delft, Z-Holland, 2628 CD, the Netherlands
[4]Mice BV, Schweitzerlaan 18, Eindhoven, N-Brabant, 5644 DL, the Netherlands
email: D.Laro@MI-Partners.nl

Abstract

In precision machines well designed vibration isolation systems isolate the accurate machine components from the surroundings, while at the same time suppressing reaction forces originating in the positioning systems of the machine itself. The isolation function requires an actuator with a low stiffness. For a machine with high accelerations, these reaction forces can typically go up to 300 N. The suppression of reaction forces demands an actuator capable of generating equally large reaction forces. Next to this the actuators dissipation should be minimised to limit thermal load on accurate machine components. A new linear actuator is developed capable of meeting all three requirements.

1 Introduction

Passive vibration isolation systems isolate the precision machine from floor vibrations. Such isolation is required to achieve sub-micrometre positioning performance. The passive vibration isolation is generally formed by a low frequency suspension, created through a mechanical or pneumatic mount. The drawback of passive vibration isolation systems is the susceptibility of these systems to reaction forces created by the positioning systems on the isolated platform. Active vibration isolation systems overcome this limitation. In active vibration isolation systems the absolute motion of the frame is measured and compensated with an active feedback loop. Actuators for active vibration isolation systems are generally voice-coil/Lorentz actuators, because of their low intrinsic stiffness. This low stiffness minimises the transfer of disturbances from the environment. However, the disadvantage of this actuator is the low efficiency, resulting in relatively large actuators or large power dissipation and accompanying heat generation. The hybrid actuator [1] excels in a high force density and low power dissipation. However, the actuator suffers from a negative stiffness, caused by the attractive forces between mover and stator, resulting in an undesired transfer of disturbances. A new design is introduced where the negative stiffness is largely compensated by a mechanical spring as presented in the next section.

2 Stiffness compensated hybrid actuator

Figure 1 shows the magnetic layout of the hybrid actuator [1]. On the stator a permanent magnet and the coils are situated. The mover consists of soft magnetic material. The permanent magnet generates a bias flux which can be manipulated with the actuation coils. This leads to a force on the mover. The permanent magnet allows efficient actuation, but also introduces a negative stiffness between the mover and the stator.

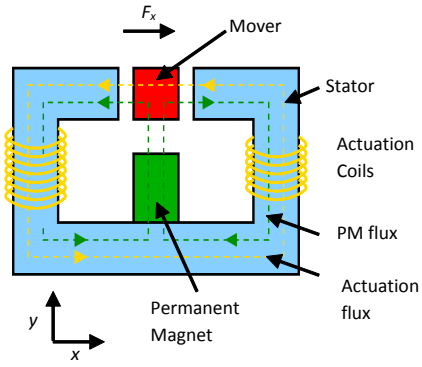

Figure 1: Hybrid actuator creates a force in x direction on the mover. The permanent magnet generates a bias flux which can be manipulated with the coils.

A plate spring parallel guide is well known in precision mechanics to facilitate motion in 1 linear direction while constraining motion in the other directions. The plate spring parallel guide has an intrinsic positive stiffness. This stiffness can be matched to compensate the negative stiffness of the actuator, resulting in a close zero stiffness actuator.

The schematic layout of the hybrid actuator with compensating plate spring is shown in Fig 2. A stinger can be used to transfer the force or displacement to an isolated platform.

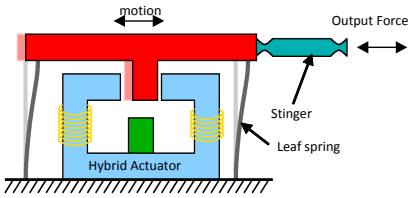

Figure 2: Hybrid actuator with a parallel plate spring guide to compensate for actuator stiffness and to constrain the other 5 Degrees of Freedom. The stinger transfers the force to the isolated platform

The remaining stiffness should be low enough, such that the actuator can be used for a vibration isolation system. Typically a vibration isolation system has a mass of 1000 kg suspended at a suspension frequency of 5 Hz. The platform's suspension stiffness is then estimated by (1).

$$k = m \cdot (2\pi \cdot f_{susp})^2 \approx 1 \cdot 10^6 \,\mathrm{N/m} \qquad (1)$$

When it is assumed that the actuator stiffness may only lead to an increase in the suspension frequency of 10%, the maximum stiffness of the actuator should not exceed 20% of the suspension stiffness. The stiffness of the actuator should be less than $2 \cdot 10^5\,\mathrm{N/m}$.

2.1 Actuator design

To cancel the reaction force of the positioning system effectively a force of 300 N is required. The stroke of the actuator is $\pm 1\,\mathrm{mm}$ since the relative displacement between the ground and the vibration isolation system is maximally $1\,\mathrm{mm}$. The geometry of the designed actuator is shown in Fig. 3.

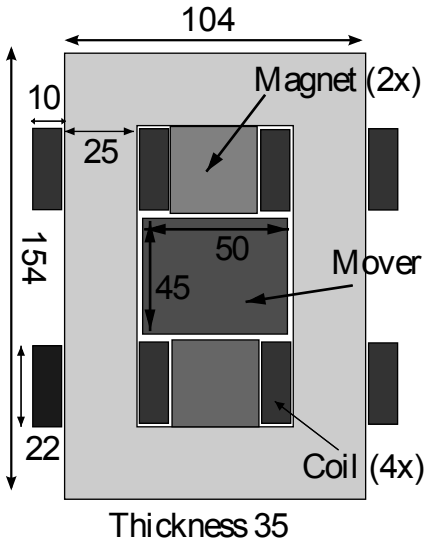

Figure 3: Dimensions of hybrid actuator to be used as reaction force cancellation actuator. The actuator is capable of generating 300 N with 300 At in total. The lamination of the stator and mover is stacked perpendicular to the image.

Compared to the design in Fig. 1 the design uses two permanent magnets to cancel the attractive force of the permanent magnet in the opposite (y) direction. Although a rotation symmetric actuator is more power efficient, a 2D structure is chosen to simplify the manufacturing and lamination of the actuator.

3 MAGNETIC DESIGN

In Fig. 4-5 the magnetic equivalent network for the hybrid actuator is shown. Such a circuit representation is only valid when the reluctance of the stator and mover is negligible, the material behaves linearly and there is no fringing flux. It is assumed the flux generated by the coils does not pass through the permanent magnet.

The reluctances of the components are given by (2).

$$R_p = \frac{l_p}{\mu_0 \mu_p A_p} \tag{2}$$

where l_p - the length of the component, μ_p - the relative permeability of the component, μ_0 - the permeability of free space and A_p - the cross section of the respective part. The sources formed by the coils and the magnet, E_{coil} and

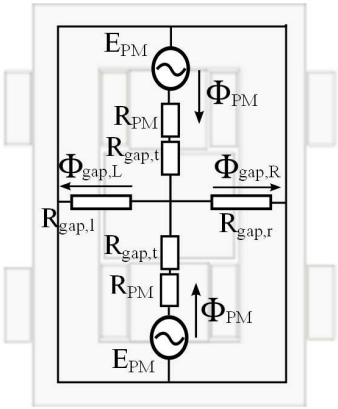

Figure 4: Magnetic equivalent network of the hybrid actuator for the permanent magnet circuit. Only the magnetic reluctances of the air gaps and permanent magnets are included, stator and mover material are assumed to have negligible reluctance.

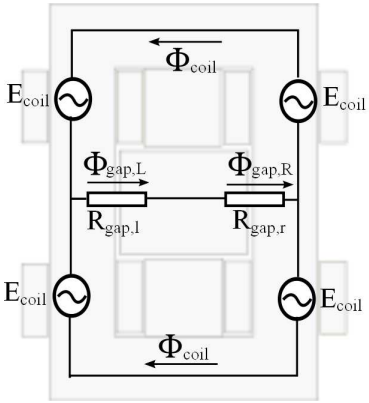

Figure 5: Magnetic equivalent network of the hybrid actuator for the coil circuit. Stator and mover material are assumed to have negligible reluctance.

E_{PM} are described by (3).

$$\begin{aligned} E_{coil} &= ni \\ E_{PM} &= H_{PM} l_{PM} \end{aligned} \tag{3}$$

where n - the number of turns per coil, i - the current through the coil, H_{PM} - the coercive force of the permanent magnet, l_{PM} - the length of the permanent magnet. Using circuit rules the magnetic flux for each source can be computed (4).

$$\begin{aligned} \Phi_{PM} &= \frac{E_{PM}}{R_{PM} + R_{gap,t} + (\frac{R_{gap,l} R_{gap,r}}{R_{gap,l} + R_{gap,r}})} \\ \Phi_{coil} &= \frac{2ni}{R_{gap,l} + R_{gap,r}} \end{aligned} \tag{4}$$

The total flux through each air gap can be computed by adding both flux paths (5). The factor two comes from the dual permanent magnet design.

$$\begin{aligned} \Phi_{gap.l} &= 2 \cdot \Phi_{PM} \cdot \frac{R_{gap.r}}{R_{gap.l} + R_{gap.r}} - 2 \cdot \Phi_{coil} \\ \Phi_{gap.r} &= 2 \cdot \Phi_{PM} \cdot \frac{R_{gap.l}}{R_{gap.l} + R_{gap.r}} + 2 \cdot \Phi_{coil} \end{aligned} \tag{5}$$

The flux density can be calculated by dividing the flux trough each air gap over its area. The force generated on the mover is equal to (6).

$$F = \frac{B_{gap.r}^2 A_{gap}}{2\mu_0} - \frac{B_{gap.l}^2 A_{gap}}{2\mu_0} \tag{6}$$

Where B_{gap} - the flux density in the air gap, A_{gap} - the area of the air gap.

The force is limited by the achievable flux density in the air gap. A limit to the air gap flux density is formed by the saturation flux density of the stator and mover material. The actuator is designed with a maximum flux density of 1.2 T in order to prevent non linearity and limit hysteresis effects in the material.

A 2D finite element model was constructed using the dimensions of Fig. 3. Figure 6 shows the force generated by the permanent magnets over the stroke of the actuator. The negative stiffness is $k_{xx} = -6.1 \cdot 10^5\,\mathrm{N/m}$. This negative stiffness will be compensated by the plate spring parallel guide as described in Sec. 4. The coils in the design are made of 1.2 mm diameter wire and have 102 turns per coil. The force generated by the coils is given in Fig. 7. The power dissipation of the actuator is 8.6 W at 3 A. Leading to an actuation constant of $10500\,\mathrm{N^2/W}$. In comparison: a commercial voice-coil actuator from Bei-Kimco type LA50-65-001Z [2] having a low stiffness and an equal volume, only has an actuation constant of $3340\,\mathrm{N^2/W}$.

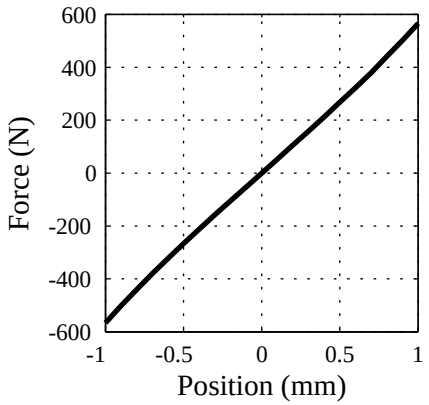

Figure 6: Negative stiffness of the magnetic design of the actuator. This stiffness will be compensated by the parallel plate spring guide.

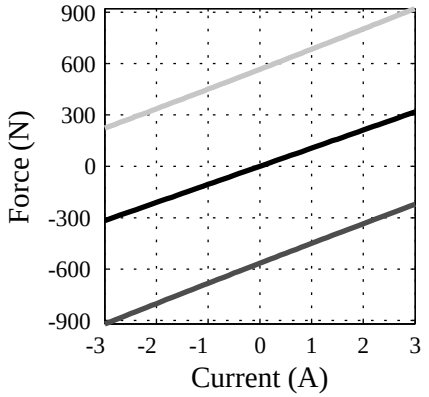

Figure 7: Force generated by the actuator. The figure shows the force with the actuator in -1 mm position (——), Actuator in 0 mm position (——), Actuator in 1 mm position (——)

In Fig. 8 the flux density of the actuator in the right air gap is shown. The flux density in the left air gap has similar values.

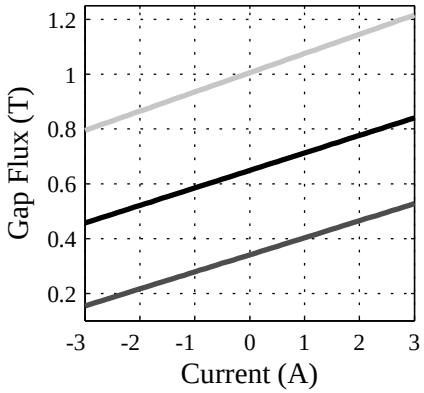

Figure 8: Flux density of the right air gap when generating the force from Fig. 7. The figure shows the flux density with the actuator in -1 mm position (——), Actuator in 0 mm position (——), Actuator in 1 mm position (——)

4 MECHANICAL DESIGN

An image of the mechanical system with plate spring parallel guide is shown in Fig. 9. The plate spring parallel guide connects the mover to the base plate. Motion in other directions than the displacement direction is constrained by the plate spring. Stiffness of the plate spring is normally kept small to reduce the required driving forces. Here the goal is to compensate the negative stiffness of the actuator. The targeted stiffness in the design is therefore $k_{xx} = 6 \cdot 10^5\,\mathrm{N/m}$. The material of the plate springs is phosphor bronze. This material is non-ferromagnetic and therefore not attracted to the hybrid actuator.

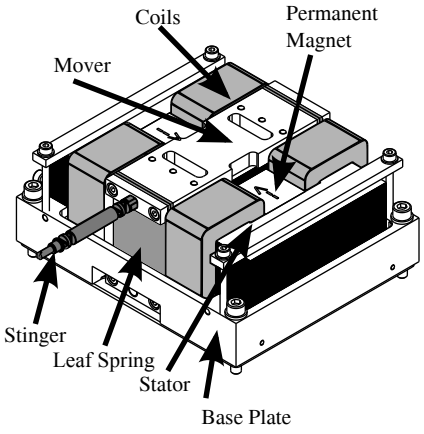

Figure 9: Hybrid actuator in its mechanical assembly. A linear encoder to measure the position of the mover is present at the bottom of the mover (not visible in image).

The stiffness of $k_{xx} = 6 \cdot 10^5\,\mathrm{N/m}$ requires a relatively thick plate spring. In order to reduce volume and keep stresses in plate springs to acceptable level in total four parallel plate springs are used. The thickness of the plate springs is chosen $1.5\,\mathrm{mm}$ to be able to use standard materials. The width of the four plate springs is $42\,\mathrm{mm}$ and the free height is $49\,\mathrm{mm}$. With these dimensions the required positive stiffness is obtained from (7) [3].

$$c_x = 2 \cdot \frac{12}{(K_y h^3)} \cdot (1 + (\frac{1}{10} F_z K_y h^2) - \frac{1}{8400}(F_z K_y h^2)^2) \tag{7}$$

where $K_y = 12\frac{1-v^2}{(2w)Et^3}$, h - the free height of the plate springs, F_z - the gravitational force on the parallel guide, v - Poisson ratio (0.3), E - Modulus of Elasticity $(115 \cdot 10^9\,\mathrm{Nm}^{-2})$, w - the width of the plate springs, t - the thickness of the plate springs.

The stiffness of the plate spring parallel guide is well matched with the negative stiffness of the permanent magnets. The thick plate springs have a maximum deflection of 1 mm. The bending stress of the plate springs is given in (8).

$$\sigma_{max} = 3E\frac{t}{l} \cdot \frac{d_x}{l} \tag{8}$$

Where d_x - the maximum deflection of 1 mm. The maximum bending stress is 215 MPa. This is just within the fatigue stress limits.

In Fig. 9 the assembled actuator is shown. The base is used to mount the stator and plate spring parallel guide. The stinger is used to transfer the forces to the payload has a high stiffness in the driving direction while having a low stiffness in the other 5 DoF. The actuator is equipped with hall sensors to measure the flux levels in the air gap.

4.1 Force measurement setup

To verify the properties of the actuator a force measurement setup is realised, Fig. 10. An ATI force sensor measures the force which is transferred through a stinger. The frame holding the force sensor can be used to position the actuator in the air gap manually.

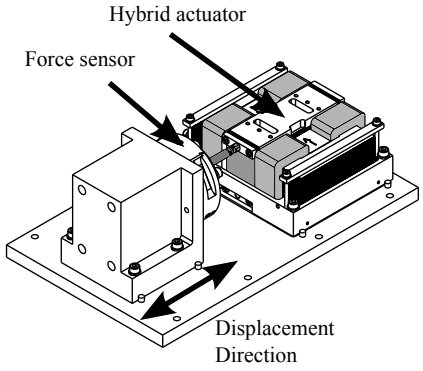

Figure 10: Setup to measure static forces of the hybrid actuator.

5 EXPERIMENTAL RESULTS

Two versions of the actuator were realised: one made of grain-oriented material, while the other was made of non-oriented material. Both versions are compared to establish which is most suitable for the application.

5.1 Static Force measurements

In Fig. 11-12 the generated force versus position is shown. The measured force is the resulting force of the plate spring parallel guide combined with the actuator itself. The stiffness of the plate spring assembly was separately measured and is $5 \cdot 10^5\,\mathrm{N/m}$. Both actuators have a hysteresis band of 30 N over a stroke of $\pm 1\,\mathrm{mm}$. The remaining stiffness for the actuators varies between $+0.5 \cdot 10^5\,\mathrm{N/m}$ for larger strokes ($> 1\,\mathrm{mm}$) and $+1.0 \cdot 10^5\,\mathrm{N/m}$ for smaller strokes ($< 0.3\,\mathrm{mm}$).

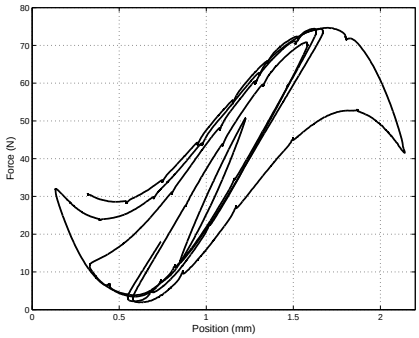

Figure 11: Position vs force close to the centre of air-gap for oriented core material, the zero position is where the actuator is stuck at end stop attached to the stator. In the center the stiffness is dominated by the plate springs and is positive.

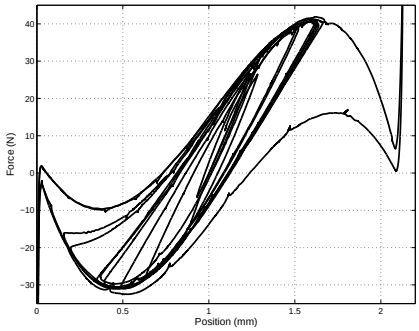

Figure 12: Position vs force at center of air-gap for non-oriented core material

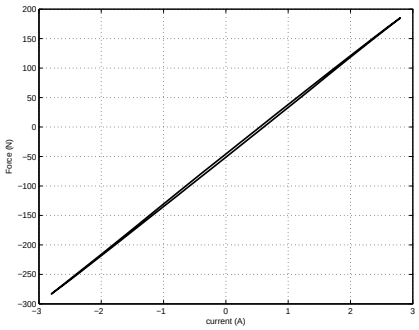

Figure 13: Current vs force at center of air-gap for oriented core material, a hysteresis band of 4 N is present

The stiffness of the plate springs will have to be reduced by $+1.0 \cdot 10^5\,\mathrm{N/m}$ to match the plate springs with the actuators and reduce the residual stiffness.

In Fig. 13-14 the actuation force over actuation current is shown. The motor constant is about 90 N/A which is 10% less than modelled. A hysteresis of band of ± 4 N is present. To establish the cause of the hysteresis the force is estimated using the integrated hall sensors. The estimated force using the hall sensors is shown in 15 and it has similar hysteresis as the measured force in Fig. 11. The hysteresis in flux density was only $\pm 2.5\,\mathrm{mT}$ however this leads to a force hysteresis of ± 4 N!

In table 1 a summary of the properties of both actua-

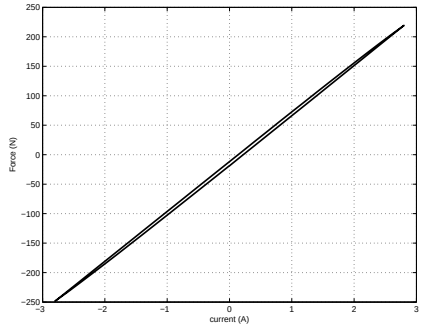

Figure 14: Current vs at center of air-gap for non-oriented core material,$5 \cdot 10^5\,\mathrm{N/m}$ is present

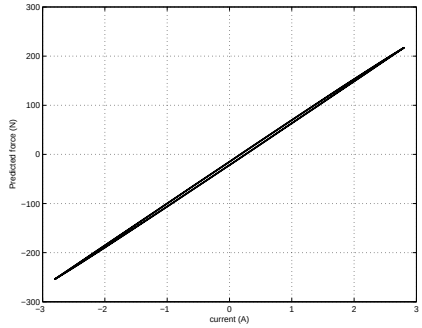

Figure 15: Force predicted using integrated hall sensors

Table 1: Actuator parameters using least square fit on 3D measurement (position, current, force)

Oriented non-oriented Core	Value
Offset force	6 N
Motor Constant	88 N/A
Average Residual Stiffness	$+4.8 \cdot 10^4\,\mathrm{N/m}$
Max. Residual Stiffness	$+1.2 \cdot 10^5\,\mathrm{N/m}$
Hysteresis band $\pm 1\,\mathrm{mm}$	29 N
Hysteresis band $\pm 250\,\mathrm{N}$	8 N
Actuator Oriented	**Value**
Offset force	50 N
Motor Constant	88 N/A
Average Residual Stiffness	$+4 \cdot 10^4\,\mathrm{N/m}$
Max. Residual Stiffness	$+1.3 \cdot 10^5\,\mathrm{N/m}$
Hysteresis band $\pm 1\,\mathrm{mm}$	30 N
Hysteresis band $\pm 250\,\mathrm{N}$	8 N

tors is given based on a least square fit over position, current and force. It is clear that both actuators are similar in performance.

5.2 Dynamic measurement

A dynamic measurement was performed to establish the applicability of the hybrid actuator in an actively controlled system or in feed-forward loop. For the actuator to function a low phase lag is desired. The FRF of the actuator is shown in Fig. 16. The resonance at 67 Hz is caused by the residual stiffness ($1.2 \cdot 10^5\,\mathrm{N/m}$) of the actuator and the mass of the mover (0.700 kg). When a better stiffness

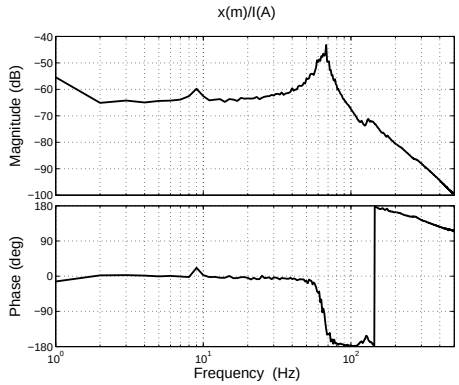

Figure 16: Plant FRF of hybrid actuator

matching or a higher moving mass is used this resonance frequency is reduced.

The phase lag of the actuator is caused by the sampling delay, the amplifier and the actuator itself. By subtracting the other two sources a phase lag of 8° can be attributed to the actuator at 200 Hz. To reduce the phase lag the current amplifier is currently being matched to the properties of the actuator.

6 CONCLUSIONS

The proposed hybrid actuator with stiffness compensation shows potential to be used in a force cancellation scheme. It has an actuation constant of $10500\,\mathrm{N^2/W}$. The residual stiffness is within specification, but improvement is desired. This can be accomplished through a better match between plate springs and actuator stiffness. Part of the stiffness mismatch will remain due to hysteresis in the magnetic materials. To reduce stiffness and hysteresis, new magnetic cores and plates spring are being manufactured.

REFERENCES

[1] X. Lu, "Electromagnetically-driven ultra-fast tool servos for diamond turning," *PhD thesis Massachusetts Institute of Technology*, 2005.

[2] Bei-Kimco, "La50-65-001z," *www.bei-kimco.com*, 2011.

[3] J. van Eijk, "On the design of plate spring mechanisms," *PhD thesis, Delft University of Technology,*, 1985.